ELSEVIER

Polymer Vol. 37 No. 13, pp. 2615–2626, 1996

0032-3861/96/$15.00 + 0.00

Morphological stability in injection-moulded high-density polyethylene/polyamide-6 blends

S. Fellahi, B. D. Favis* and B. Fisa

École Polytechnique de Montréal, Centre de Recherche Appliquée sur les Polymères, PO Box 6079, Station 'Centre-ville', Montréal, Québec H3C 3A7, Canada

(Received 18 May 1994; revised 6 March 1995)

The morphology of injection-moulded high-density polyethylene/polyamide-6 (25/75 vol%) blends, with and without compatibilizer, is investigated both throughout the sample and in the weldline region. A detailed morphological analysis of the skin and weldline using scanning electron microscopy and image analysis established: (a) a significant skin/core effect, (b) a diminution of the thickness of the skin and weldline regions with interfacial modification, and (c) an apparent absence of the minor phase in the skin and weldline. Subsequent more detailed work indicated that there was, in fact, no absence of the minor phase in the skin and weldline. The existence of a morphological variation with respect to the thickness (dispersed phase is highly oriented in the subskin and spherical in the core) is clearly shown in this study. X-ray photoelectron spectroscopy and differential scanning calorimetry of microtomed layers from the surface were used as additional techniques to show that the surface and the weldline region composition of dispersed phase is very close to the original, as-prepared, composition (25/75 vol%). Transmission electron microscopy reveals the presence of a very fine dispersed phase in the skin with particle dimensions almost one order of magnitude smaller than in the core. The interfacial modifier, a poly(ethylene–methacrylic acid–isobutyl acrylate) ionomer, was found to reduce the size of the dispersed phase, the skin thickness and the width of the weldline. The dimensions of the regions with very fine dispersed phase (skin and weldline) correlate well with those observed in the advancing melt front as analysed in the short-shot samples. Less coalescence and a more stable morphology is observed.

(Keywords: injection moulding; HDPE/PA6 blends; morphology)

INTRODUCTION

The last decade has seen intense activity to tailor new plastic materials in the form of blends or alloys using melt processing equipment. This approach has considerable cost advantages over the development of materials in polymerization reactors. Blends have an annual growth rate of about 10% compared to about 3% for plastics alone[1].

Polymer blends are mixtures of homopolymers or copolymers of different molecular structure. Immiscible polymer blends possess a minor phase that may undergo severe deformation and acquire an anisometric configuration during melt processing, resulting in a structure characterized by a distribution of shape-factor ratios, concentration and orientation of the dispersed phase throughout the thickness of a moulded part. Most industrial polymer blends are immiscible. Consequently the introduction of a compatibilizer either as a third component or developed *in situ* through reactive processing[2–4] at a reduced concentration level is necessary to reduce the interfacial tension and the dispersed phase size, to improve the adhesion and subsequently to improve the mechanical properties[5]. This will normally result in a more stable morphology[6–8].

Blends of non-polar polyolefins with polar polyamides are an example of materials where the dissimilarity of components dictates the use of a suitable compatibilizer. There have been several studies of the polyolefin/polyamide system[9–13]. White *et al.*[9] studied the rheology and the morphology of extruded polypropylene/polyamide (PP/PA), considering in particular the influence of melt temperature and polyethylene (PE) viscosity[8] and the development of different types of morphologies[10]. A comparative morphological study between compression- and injection-moulded non-compatibilized high-density polyethylene/polyamide-6 (HDPE/PA6) blends[14], in which the mould temperature, the annealing time inside the mould and the injection speed were varied, revealed the presence of the usual skin/core structure, with an oriented skin, an intermediate zone where the anisotropy is maximum and an isotropic core. The dispersed phase was found to form plaques or oriented lamellae in the machine direction.

Factors influencing the morphology of polyolefin/polyamide blends have been studied extensively in this laboratory[15–18]. The influence of interfacial modification through the use of a poly(ethylene–methacrylic acid–isobutyl acrylate) ionomer in such systems has been considered[16,17,19]. Chemical bonding was found to occur at the interface through amide formation between the

* To whom correspondence should be addressed

carbonyl group of the ionomer and the terminal amine of polyamide. It has been shown that interfacial modification in these systems can significantly diminish the phase size/volume fraction dependence. Hence coalescence effects are reduced and morphological stability is enhanced[1,3,5]. Despite this work and others[14] on polyolefin/polyamide blends, very few studies have considered the morphology developed during injection moulding.

Injection moulding is characterized by a complex and non-isothermal flow in a closed and cooled mould cavity. This generally results in an anisotropic skin/core structure. The filling of the mould cavity occurs through fountain flow. During moulding, the plastic in contact with the cooled mould wall will freeze immediately to form the skin where the shear will be maximum. Dispersed, deformable polyethylene particles will be elongated in the direction of flow. The hot core will be less deformed, and has sufficient time to relax. The final result of this complex process is the so-called skin/core morphology.

Weldlines

When two separate polymer flow fronts come into contact, a zone called a 'weldline' or 'knit line' having a morphology and properties different from the rest of the material is formed. Weldlines produced by the separation and recombination of the flow around an insert represent the most frequently encountered situation in industrial parts[20].

Weldlines in homopolymers is a well documented subject[20–28]. The quality of a weldline is associated with the flow field that arises as the two fronts reunite. A possible explanation for the weakness engendered by this reunion is the trapped air at the interface between the two opposing fronts, leading to the formation of a V-notch that can act as a stress concentrator[21,22]. Tadmor[23] proposed that such flows generate molecular orientation that is predominantly along, rather than across, the weld interface because of a fountain-like flow. Two processes that most likely precede the weld healing are stress relaxation, which results in a loss of this orientation, and molecular re-entanglement, which is a self-diffusion phenomenon. A stress relaxation mechanism has been invoked by Tomari *et al.*[24], while the latter process has been adopted by De Gennes[25] and Wool *et al.*[26], to explain the healing phenomenon. Finally, Titomanlio *et al.*[27] have used the volume shrinkage approach to explain the weakness due to the presence of a weldline.

Weldlines in injection-moulded polymer blends is not a well documented subject. Injection-moulded ethylene–propylene–diene monomer/polypropylene (EPDM/PP) systems with a weldline obtained with a double gated mould were studied by Thamm *et al.*[29]. They reported an absence of the minor phase (EPDM) in the weldline region. When the viscosity of the EPDM was lower than that of the PP, the former was found to migrate to the surface. Similar results were reported later by Malguarnera *et al.*[28]. They attributed the absence of the dispersed EPDM in the weldline region to a deficiency in the flow-front region, although this was never supported experimentally. Paul *et al.*[30] have studied the effect of a compatibilizer on the mechanical properties of several systems with and without weldline obtained in a double gated mould. Karger-Kocsis *et al.*[31] studied the structure–properties relationships and the phenomena causing rupture of injection-moulded blends of EPDM/PP with and without a weldline obtained by double gate feeding. The usual skin/core structure was found. In the skin, two zones were observed: a thin PP layer on the surface, and a subskin with highly elongated rubber particles. The core was rich in rubber particles. This effect was attributed to the existence of a concentration gradient due to crystallization of the front in contact with the mould surface. During crystallization the polypropylene apparently rejects the rubber particles instead of engulfing them.

Preliminary morphological observations were also carried out in studies on HDPE/PA6 compatibilized with an ionomer[32,33]. Significant morphological and concentration variations throughout the thickness of the plaque are reported. A deficiency of the minor phase in the skin and weldline region was also discussed[33].

One of the main concerns in the processing of polymer blends is the stability of the morphology. It is generally believed that the addition of an interfacial modifier leads to a better stabilization of the morphology. Despite this fact, little detailed work has been undertaken on the morphology of both compatibilized and non-compatibilized blends during injection moulding and including weldlines.

The objective of the present work is to consider the effect of a poly(ethylene–methacrylic acid–isobutyl acrylate) ionomer on the morphological characteristics of injection-moulded HDPE/PA6 systems including weldlines. A detailed morphological analysis of the skin and weldline will be undertaken by scanning electron microscopy (SEM), transmission electron microscopy (TEM) and image analysis. Since both the skin and the weldline region originate from the flow front, a morphological analysis of the latter will also be carried out. X-ray photoelectron spectroscopy (X.p.s.) and differential scanning calorimetry (d.s.c.) of microtomed layers from the surface will be used as additional techniques to characterize qualitatively and quantitatively the surface and the flow-front composition of the plaques.

EXPERIMENTAL

Materials

The polyamide-6 (PA6) is a Zytel 211 from E. I. du Pont de Nemours & Co. Inc. with a number-average molecular weight $M_n = 25\,000\,g\,mol^{-1}$. The high-density polyethylene (06153C) is from Dow Chemical Canada having a melt flow index MFI = 6.3 g/10 min, $M_n = 20\,200\,g\,mol^{-1}$ and $M_w = 81\,300\,g\,mol^{-1}$. The compatibilizing agent is an ionomer (Surlyn 9020, from E. I. du Pont de Nemours & Co. Inc.), a terpolymer consisting of 80% ethylene and 20% mixture of methacrylic acid and isobutyl acrylate. The methacrylic acid is 70% zinc neutralized, having a molecular weight $M_n = 25\,000\,g\,mol^{-1}$ (obtained from the supplier). The polyethylene is stabilized with 0.2% antioxidant (Irganox 1010 of Ciba Geigy).

Compounding

The first operation consisted of mixing polyethylene (HDPE) with 0.2 wt % antioxidant (Irganox) in a single-screw extruder. Then, using a twin-screw extruder, 10% ionomer (I), based on the weight of the dispersed phase, was mixed with the stabilized PE. Finally, 25 vol% of PE

Table 1 Compounding conditions

	PE/antioxidant			PE/ionomer			PEIPA[a]			PEPA[b]		
		25 kg PE 50 g antioxid			10 kg PE 1.11 kg I			12 kg PA6 3.083 kg PE/I			2.793 kg PE 10.87 kg PA	
	Fixed	single screw	Obs	Fixed	twin screw	Obs	Fixed	twin screw	Obs	Fixed	twin screw	Obs
T_1 (°C)	160		146	160		152	185		180	185		180
T_2 (°C)	170		165	185		188	235		232	235		235
T_3 (°C)	180		170	190		203	250		245	250		235
T_4 (°C)		175		195		212	250		250	245		233
T_5 (°C)		180		195		192	245		240	245		233
T_6 (°C)		190		200		201	250		240	250		230
Rpm		80			300			300			200	
Flow rate (g min^{-1})		90			170			180			100	
Torque (%)					65			65			50	
Feeding under N_2		No			Yes			Yes			Yes	
Degassing		No			Yes			Yes			Yes	

[a] (Stabilized polyethylene/ionomeric compatibilizer)/polyamide-6
[b] Stabilized polyethylene/polyamide-6

with (PEIPA) or without compatibilizer (PEPA) was mixed with 75 vol% of polyamide (PA6). Prior to a typical mixing operation, the sample mixture was dried overnight at 90°C under vacuum to minimize hydrolytic degradation of the polyamide during processing. The polymer blending was carried out on a ZSK-30 (Werner-Pfleiderer) intermeshing, co-rotating twin-screw extruder with a screw length-to-diameter ratio L/D of 40. Feeding was performed under nitrogen and vacuum was applied in the decompression zone. The blending conditions are shown in *Table 1*. Rod-shaped extrudates were kept for SEM observation.

Rheology

The viscosities of all pure materials (HDPE, ionomer and PA6) and the two prepared formulations (PEPA and PEIPA) were measured at 200, 230 and 250°C using three dies having different L/D ratios of 10, 20 and 40 on an Instron capillary viscometer. Only data at $L/D = 40$ and 250°C will be reported here.

Injection moulding

The injection moulding machine used was a Battenfeld type BA-C 750/300, with a clamping force of 80 tons (~710 kN). A conventional mould equipped with interchangeable cavities of rectangular shape (127 mm × 76 mm × 4 mm) was used. It is equipped with a 2 mm deep flash gate fed with a trapezoidal duct having a section varying from 30 to 50 mm^2 (*Figure 1A*). To produce plaques with weldlines, an insert having 12 mm diameter is installed in the cavity (*Figure 1B*).

Four types of experiments were performed: full plaques and short shots both with and without insert, using the previously prepared formulations. The injection moulding conditions are:

thickness of the plaque = 4 mm
insert diameter = 12 mm
shot weight = 50.2 g
total cycle time = 42 s
cooling time = 20 s
hold time = 10 s
nozzle temperature = 250°C
mould temperature = 65°C
injection pressure = 150 bar
hold pressure = 100 bar
screw speed = 50 rpm
injection speed = 100 mm s^{-1}
materials dried in air circulating oven at 80°C

Morphological analysis

Electron microscopy. In addition to the twin-screw extrudates, samples were taken at different positions from complete injection-moulded (transversely and longitudinally to flow direction) and short-shot plaques as indicated in *Figure 1B*, according to the preceding conditions. Only formulations of (25/75) PE/PA6 with and without compatibilizer were studied. Morphological preparation can proceed in two ways.

(i) *Freeze-fracture*: A small circular or rectangular

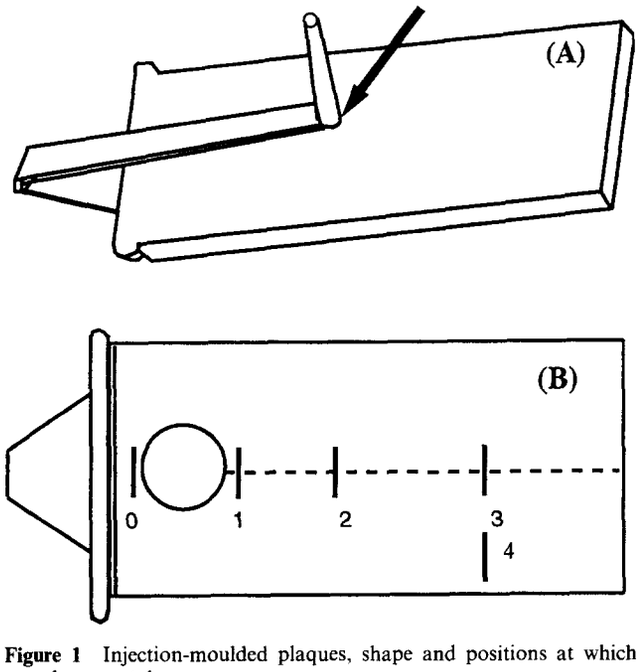

Figure 1 Injection-moulded plaques, shape and positions at which samples were taken

strip from each sample is placed in liquid nitrogen for 10–15 min, and then fractured manually.

(ii) *Microtoming*: Rectangular samples ($1 \times 1.5 \times 0.5\,cm^3$) were cut. A Reichert Jung Supercut 2050 microtome equipped with a glass knife was used. First, each sample was frozen in liquid nitrogen for 15 min. During the cutting operation, the temperature was kept at approximately $-100°C$ to reduce the extent of surface deformation. The microtomed samples were immersed for 1 h in decalin at 120°C to dissolve the polyethylene (minor phase). Following the extraction the samples were dried in a vacuum oven for 24 h to remove the solvent.

Freeze-fractured or microtomed surfaces were then treated with a gold–palladium layer and examined in a JEOL 8645 type scanning electron microscope.

Image analysis. The semi-automatic image analyser used to measure the diameters of the dispersed phase was the Jandel digitizing tablet controlled by the Jandel Sigma-scan system. For each sample, approximately 300 diameter measurements on one run were obtained from the SEM micrographs. The experimental error was approximately ±10%. When the same measurements were carried out successively on the same micrograph, the difference was less than 10%. A correction was applied to the distribution of diameters for each sample according to the Saltikov method. The mathematical particle corrections account for two phenomena: (a) the fact that the observed diameter of a given particle, after microtoming or fracture, is usually less than the true diameter of the original spherical particle; and (b) materials with large dispersed particle size distributions result in an average diameter value that overestimates the contribution of large particles[34].

Transmission electron microscopy. Slices of less than 80 nm thickness were cut using an ultramicrotome type RMC-MT-7 at a 30° angle of inclination, and a cutting speed of $2\,mm\,s^{-1}$ from the skin region in both directions (transverse and longitudinal to flow) of PA6, HDPE and PEPA plaques to a depth not exceeding 80 μm. They were then observed under a JEOL 2000FX transmission electron microscope with a voltage of 200 kV.

Differential scanning calorimetry

A DuPont 900 differential scanning calorimeter was used with a scanning rate of $20°C\,min^{-1}$. Samples from neat HDPE, neat PA6 and PEPA blend were microtomed from the surface of the plaques to a depth not exceeding 100 μm.

X-ray photoelectron spectroscopy

Samples (5 mm × mm) were cut from neat HDPE, PA6, PEPA, Surlyn and PEIPA plaques, as well as from the flow front on a non-compatibilized blend. They were then surface analysed using X-ray photoelectron spectroscopy (X.p.s.). X.p.s. studies were carried out on a VG Escalab MkII instrument. An X-ray beam (Mg Kα at 1253.6 eV) was used to produce the photoemission of electrons from core and valence levels of the surface atoms. About 60 Å of depth were probed, when the detector was perpendicular to the surface. The analysed surface was 2 mm × 3 mm. All peak positions were corrected for adventitious carbon, at 285.0 eV in binding energy, to adjust for charging effect. The results obtained with this technique are reported[35] to be accurate within ±5%.

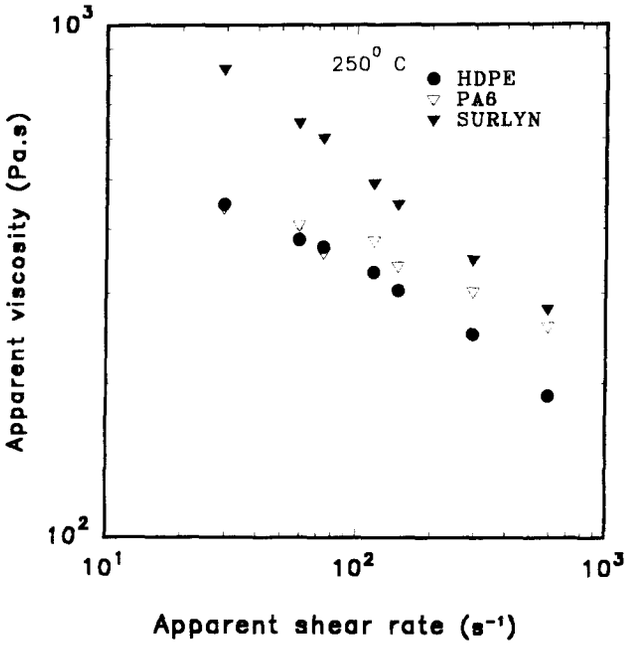

Figure 2 Apparent viscosity vs. shear rate of neat HDPE, PA6 and Surlyn

RESULTS AND DISCUSSION: RHEOLOGY

From *Figure 2*, it can be seen that the polyamide (PA6) has a somewhat higher viscosity than the polyethylene (PE) over the range of shear rates considered. Since the viscosity ratio at high shear rates is slightly less than 1, this should ensure a fine dispersion[36]. It can be noticed that the compatibilizer (Surlyn) has a higher viscosity than the other components.

In *Figure 3*, the viscosity of the PEPA blend shows a negative deviation with respect to that of pure PA6. The presence of HDPE causes a drastic reduction in the PA6

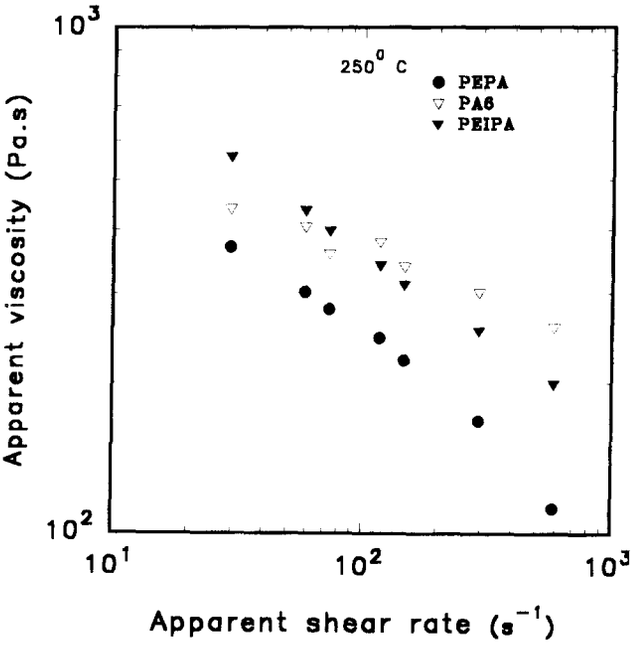

Figure 3 Apparent viscosity vs. shear rate of neat PA6, uncompatibilized (PEPA) and compatibilized (PEIPA)

viscosity. When a compatibilizer is used, the system PEIPA shows a positive deviation from additivity at low shear rates (below $100\,s^{-1}$) and a negative one at higher shear rates with respect to PA6. The increase in viscosity is attributed to interfacial interactions[16].

RESULTS AND DISCUSSION: MORPHOLOGY

In the following discussion, morphological results on samples taken from extrudates (twin-screw extrusion), sprue area and inside the mould cavity (injection moulding) will be presented.

Twin-screw extrusion

Table 2 shows the influence of twin-screw processing on the size of the dispersed phase. Twin-screw extrudates display small particles located at the skin ($d_v = 1.60\,\mu m$), while the core of the sample consists of coarser particles ($d_v = 5.0\,\mu m$) for the non-compatibilized blend. When a compatibilizer is added, the size of the dispersed phase is reduced in both the skin ($d_v = 1.40\,\mu m$) and core $d_v = 1.20\,\mu m$), and a more uniform distribution of the dispersed phase throughout the sample cross-section is observed.

Injection moulding

Sprue area. In the sprue area (position indicated in *Figure 1*), a uniform distribution of the dispersed phase is observed. The shear rate in the gate is between 300 and $400\,s^{-1}$. The sprue area is not cooled except at its bottom, and the sample to be analysed was cut at this position. When the extruded compound is injection moulded a cross-section of freeze-fractured sprue reveals a finer skin and a coarser core for both blends as compared to the twin-screw extruded samples. Results are shown in *Table 2*. Overall, the injection moulding step causes an additional but slight reduction of the dispersed phase size, which might be attributed to the high shear-rate level developed in the sprue region. For the non-compatibilized blend a coarse structure throughout the cross-section ($d_n = 2.50\,\mu m$ and $d_v = 4.0\,\mu m$) is observed. When a compatibilizer is added, the structure is much finer in both the skin ($d_n = 0.30\,\mu m$ and $d_v = 0.40\,\mu m$) and the core ($d_n = 0.71\,\mu m$ and $d_v = 0.90\,\mu m$). When the system is compatibilized, a much finer dispersion is observed and this is attributed to interfacial interactions[16].

Skin/core region. Inside the mould cavity, the usual skin/core morphology is found. As the molten material enters the cavity in a parabolic profile, and the material in the front is deposited on the wall undergoing considerable stretching, it solidifies instantaneously forming an immobile frozen layer. The additional molten material will flow inside this envelope. It is well known that the velocity is at a maximum in the core and nil at the wall (*Figure 4*). The shear stress shows the opposite tendency; a maximum at the skin and a minimum in the core[23]. Because of the high shear encountered in this process, the material is highly pseudoplastic, meaning that the velocity profile is quite flat, and only a thin region in the vicinity of the frozen layer (subskin) will be highly elongated[37]. The core region will be the last to solidify, and may even relax[20]. The skin region was also observed at higher magnification (×10 000) on the SEM; however, no dispersed phase was evidenced. Selective solvent

Table 2 Comparison of the dispersed phase size[a] (μm): d_n and d_v

		PEPA[b]			PEIPA[c]		
		d_n	d_v	d_v/d_n	d_n	d_v	d_v/d_n
Twin-screw extruder (extrudate)	Skin	1.0	1.6	1.6	0.91	1.40	1.5
	Core	2.7	5.0	1.8	0.91	1.20	1.3
Injection moulding (sprue)	Skin	2.5	4.0	1.6	0.30	0.40	1.3
	Core	2.6	3.9	1.2	0.71	0.90	1.3

[a] Diameters: d_n = number-average value; d_v = volume-average value
[b] Non-compatibilized HDPE/PA6
[c] Compatibilized HDPE/ionomer/PA6

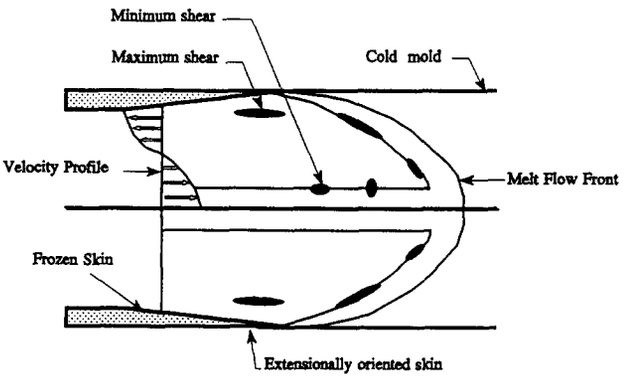

Figure 4 Schematic representation of the fountain flow

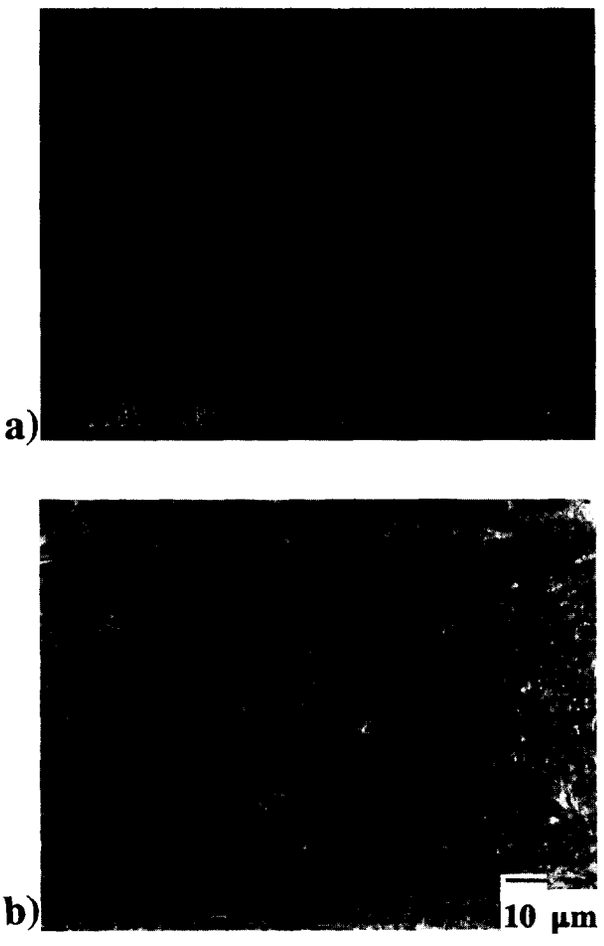

Figure 5 Morphology of non-compatibilized sample. (a) Morphological change throughout the thickness in complete sample at position 4 (parallel to flow view). (b) Shear-induced coalescence in the subskin region of a non-compatibilized sample (perpendicular to flow view)

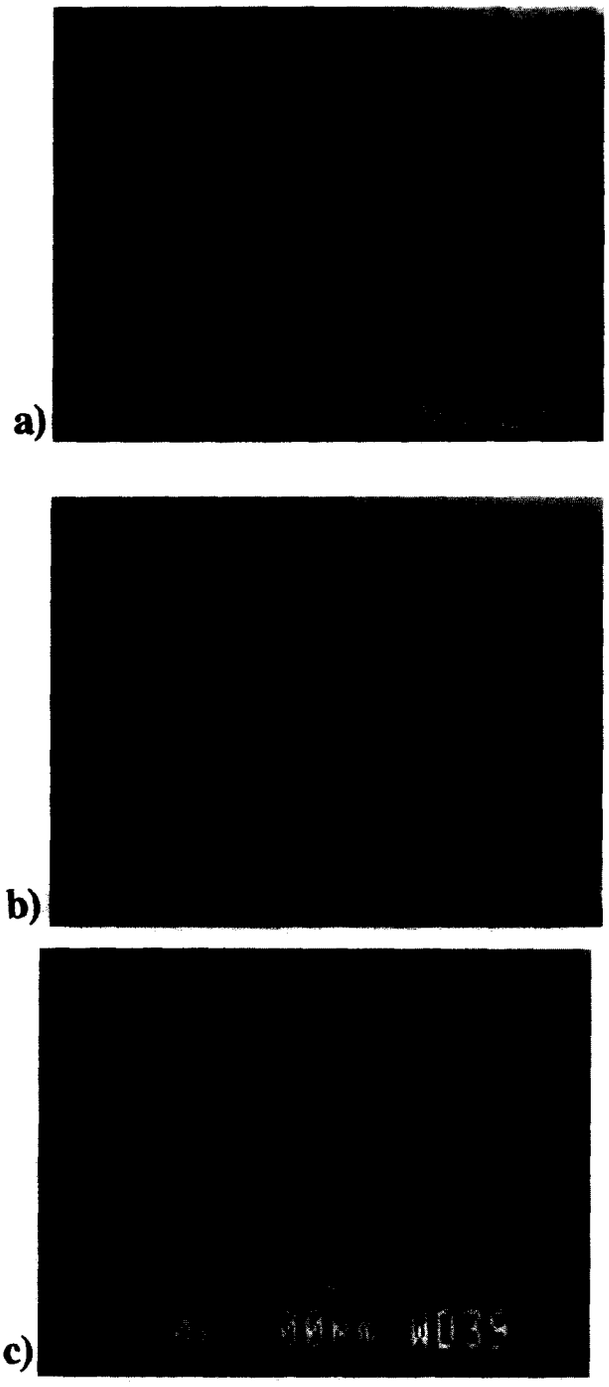

Figure 6 Morphological change throughout the thickness: (a) compatibilized complete sample at position 4 (parallel to flow view); (b) compatibilized complete sample at position 2 (perpendicular to flow view); (c) magnification in the subskin region of (a)

dissolution of the sample indicates that the skin is apparently composed of pure PA6 (*Figures 5* and *6*). The subskin is rich in PE where apparently shear-induced coalescence has taken place. For the non-compatibilized systems (*Figure 5*) the skin and the subskin are approximately 300 and 600 μm thick respectively. A highly oriented subskin region and shear-induced coalescence are observed (*Figure 5b*). When a compatibilizer is used, the morphology is more stable, and less elongation is observed (*Figures 6a–c*) in the subskin region. The skin and the subskin in this blend are approximately 100 and 400 μm thick respectively. The delineation between the different zones is relatively simple. It is based on the

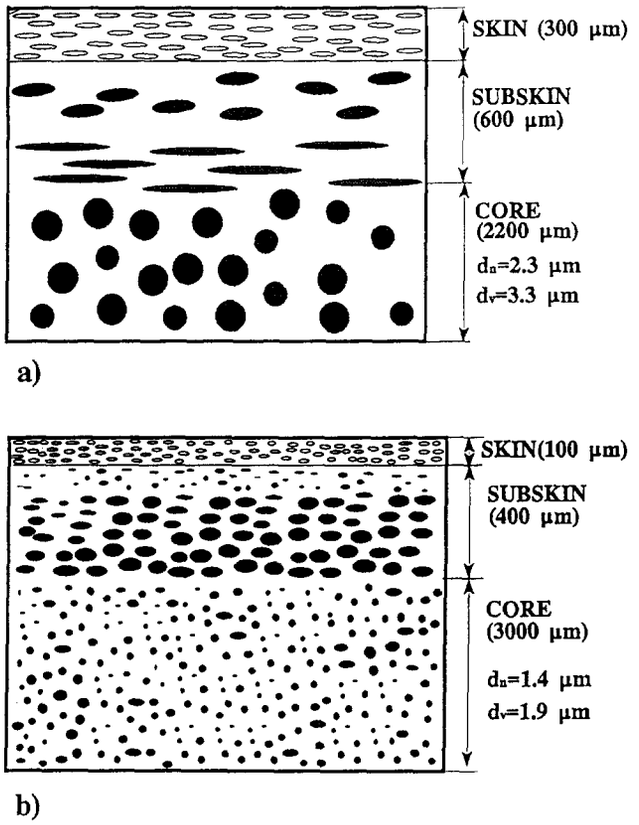

Figure 7 Schematic of the skin/core structure of injection-moulded parts: (a) non-compatibilized blend; (b) compatibilized blend

discontinuity between very small (in the skin and the weldline region) and very large particles elsewhere (subskin and core). A detailed schematic representation of the observed morphology for both blends is illustrated in *Figure 7*. The principal features of the above micrographs are the following:

(i) Significant skin/core effect observed for non-compatibilized blends displaying a morphological variation with respect to the thickness, i.e. dispersed phase is very fine in the skin, highly oriented in the subskin and spherical in the core.

(ii) Diminution of the thickness of the skin and weldline regions with interfacial modification displaying a reduced minor phase size.

(iii) Apparent absence of the minor phase in the skin even at higher SEM magnification.

To check the validity of the above observation related to the apparent absence of dispersed phase, d.s.c. thermograms of microtomed slices from the skin, transmission electron microscopy (TEM) as well as X-ray photoelectron spectroscopy of the surface of the blends, Surlyn and neat resins were performed. If the skin of the plaques made of the non-compatibilized blend as already reported above is made of pure PA6, then, when an 80 μm layer is microtomed from this region and analysed by d.s.c., it should reveal only the presence of a PA6 melting peak (220°C). As shown in *Figure 8* this was not the case. Both phases are clearly present in the skin. The test was repeated several times to ensure reproducibility, and it is evident that, in the skin, the dispersed phase is present (T_{melt} = 130°C), which apparently contradicts the SEM results. Thermograms of samples taken from the skin region for neat HDPE, PA6 and the blend are shown in *Figure 8* (curves 1, 2 and 3 respectively). The

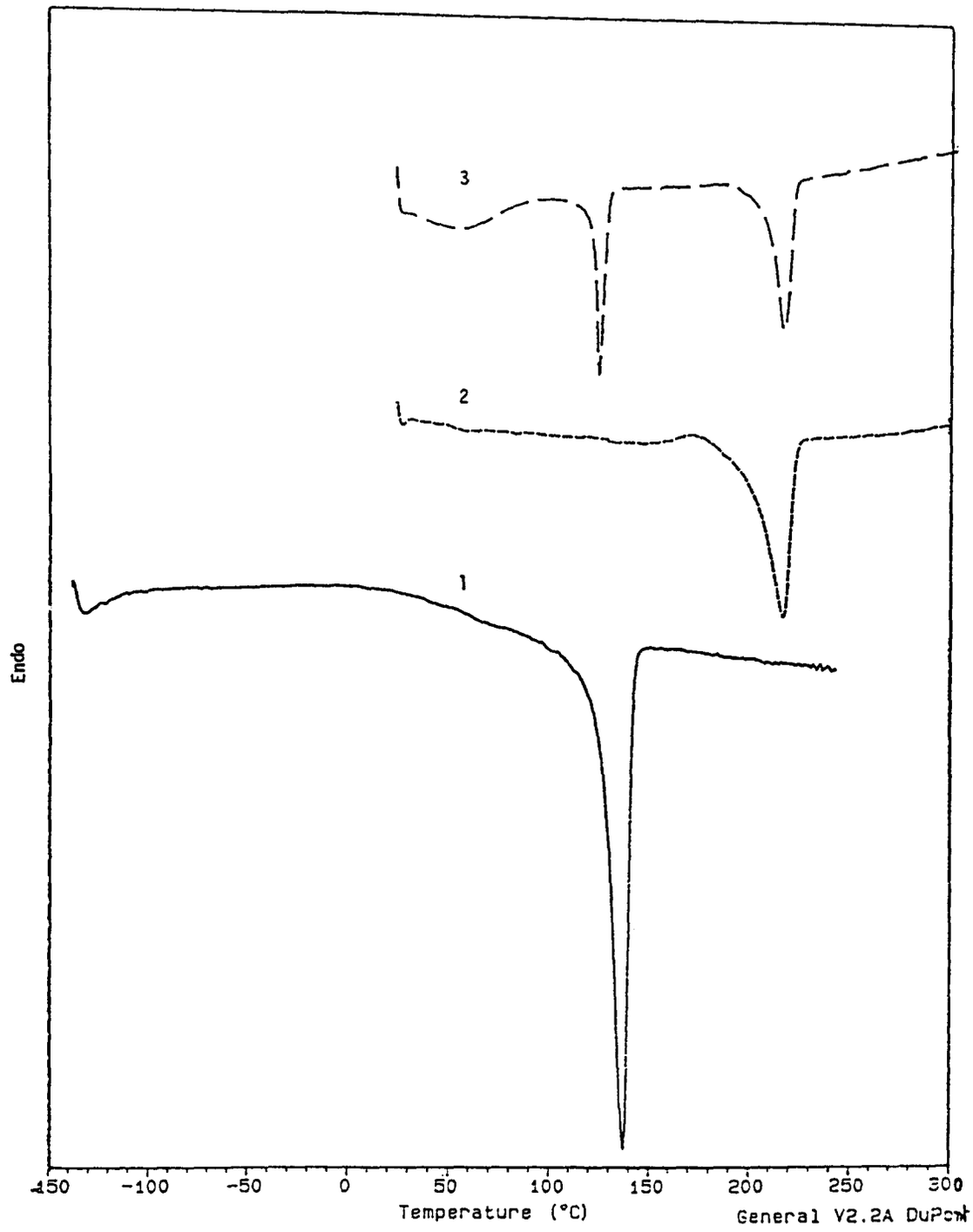

Figure 8 D.s.c. thermograms for: (1) HDPE, (2) PA6 and (3) PEPA (samples taken from the skin)

areas under their respective peaks indicate that approximately the same proportions (21.7 wt%/78.3 wt%) of HDPE/PA6 exist in the blend skin as in the original, as-prepared compound (20.4/79.6 wt%). The area under the peak in neat HDPE is $168\,J\,g^{-1}$ and in neat PA6 is $72\,J\,g^{-1}$. For the non-compatibilized blend (PEPA) under investigation, the area under the peak corresponding to PE is estimated to be $29\,J\,g^{-1}$ while that for PA6 is $44\,J\,g^{-1}$. To predict the percentage composition of the blend skin, a rule of mixtures approach was applied to the area under the peaks.

In order to verify the surface composition of the blend, another technique, X-ray photoelectron spectroscopy (X.p.s.), was carried out. This technique, also known as electron spectroscopy for chemical analysis (e.s.c.a.), is widely used to investigate the chemical composition of surfaces. Surface analysis by X.p.s. involves irradiating a solid *in vacuo* with monoenergetic soft X-rays and analysing the emitted electrons by energy. The spectrum is obtained as a plot of the number of detected electrons per energy interval *versus* their binding energy. The detected electrons originate from only the top few atomic layers, making X.p.s. a unique surface-sensitive technique for chemical analysis[38]. Since the percentages of carbon atoms of pure HDPE and nylon are different, the percentage of carbon atoms obtained by X.p.s. can give an indication of the relative proportion of a given component. The spectra of neat HDPE, PA6 and Surlyn

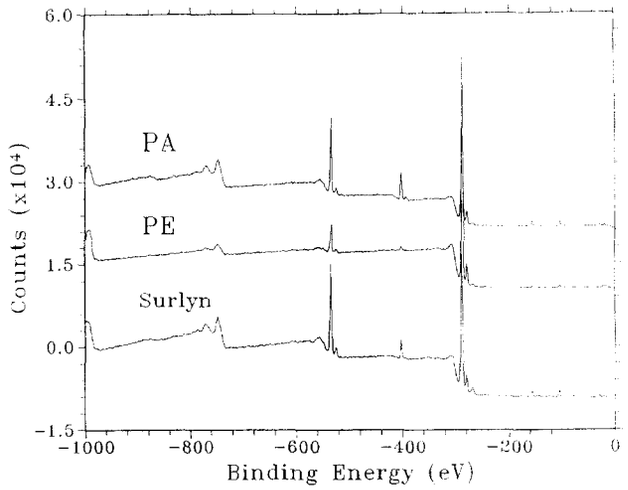

Figure 9 X.p.s. spectra from the surface of PA6, HDPE and Surlyn plaques

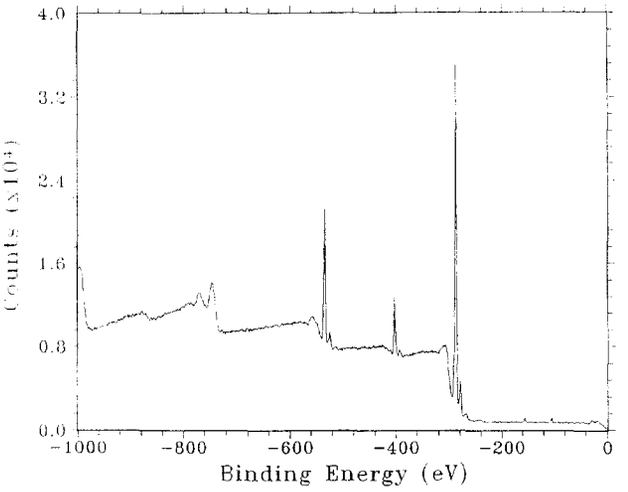

Figure 11 X.p.s. spectrum from the surface of compatibilized blend

are shown in *Figure 9*, while those of the blends are shown in *Figures 10* and *11*. The results are summarized in *Table 3*. It can be seen that the carbon atoms amount to 71.9% (here % stands for at%) for neat PA6 and 92% for neat HDPE. The lower percentage value for PA6 is related to the presence of other atoms such as nitrogen and oxygen in PA6. In neat HDPE, there is 6.2% oxygen. This can be attributed to carbonyl groups formed during the polymerization reaction[39]. The non-compatibilized blend reveals the presence of 77.8% carbon (C) atoms, 7.1% nitrogen (N) atoms and 13.1% oxygen (O) atoms. Knowing the percentages of C, N and O for the neat components as well as that for the blend, the blend skin composition can be estimated via a rule of mixtures approach. These results confirm that the skin exists as a blend at approximately the same composition (24.4 wt% HDPE/75.6 wt% PA6) as in the original, as-prepared, blend (20.4 wt% HDPE/79.6 wt% PA6). Similar observations also hold true for the compatibilized system. No segregation of individual blend components occurs. The X.p.s. data therefore confirm the d.s.c. results.

Finally, TEM observations on very thin slices (80 nm) cut from the skin region of the plaque in the direction perpendicular (*Figure 12a*) and longitudinal to flow (*Figure 12b*) revealed the presence of highly oriented HDPE particles, having an average diameter less than 0.5 μm and a length between 5 and 10 μm. These results therefore indicate the presence of a very fine and elongated dispersed phase in the skin. The TEM studies of the non-compatibilized system indicate the presence of very fine dispersed phase structures of less than 0.5 μm thickness. It should be noted that these dimensions are almost one order of magnitude smaller than that observed in the core of the sample. The transverse section (taken perpendicular to the flow direction) illustrates that ribbon-like structures exist in the skin and demonstrates the presence of significant biaxial stretching.

It is clear therefore that the apparent absence of dispersed phase as observed by SEM and shown in *Figures 5* and *6* can be attributed to the very fine size of the dispersed phase in the skin relative to the core. During SEM analysis typical magnifications used to evidence the core structure are not sufficiently high enough to allow visualization of the skin region. In fact d.s.c. and X.p.s. results show the surface composition of the dispersed phase to be very close to the original, as-prepared, composition. Transmission electron microscopy further illustrates that the dispersed phase in the skin is very small and highly elongated.

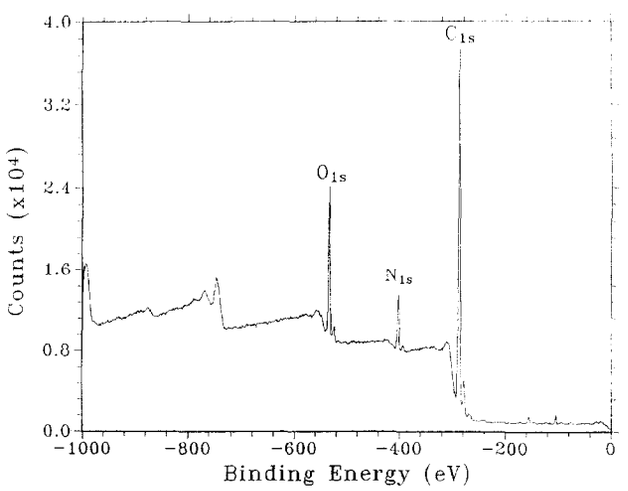

Figure 10 X.p.s. spectrum from the surface of non-compatibilized blend

Core. The core represents approximately 50% of the whole sample in the non-compatibilized blend and 75% in the compatibilized one. The dispersed phase particles are more spherical than elsewhere, owing to relaxation occurring during the cooling process. The structure of the core is coarser ($d_n = 2.30\,\mu$m and $d_v = 3.30\,\mu$m) with loose particles and is 2200 μm thick for the uncompatibilized blend. The compatibilized blend displays a

Table 3 Composition of the surface of the plaques as revealed by X-ray photoelectron spectroscopy (X.p.s.)

	Carbon (at%)	Nitrogen (at%)	Oxygen (at%)
PA6	71.9	8.4	16.1
HDPE	92.0	0.8	6.2
Surlyn	76.2	4.2	16.6
PEPA	77.8	7.1	13.5
PEPA front	78.6	1.8	12.6
PEIPA	79.8	7.0	12.0

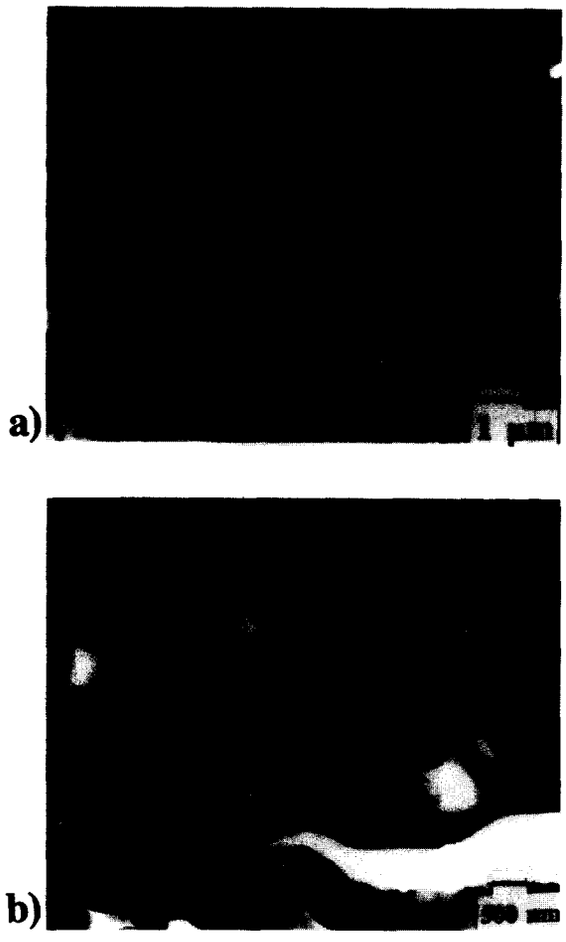

Figure 12 TEM micrographs of samples taken from the skin region of: (a) PEPA transverse view; (b) PEPA longitudinal view

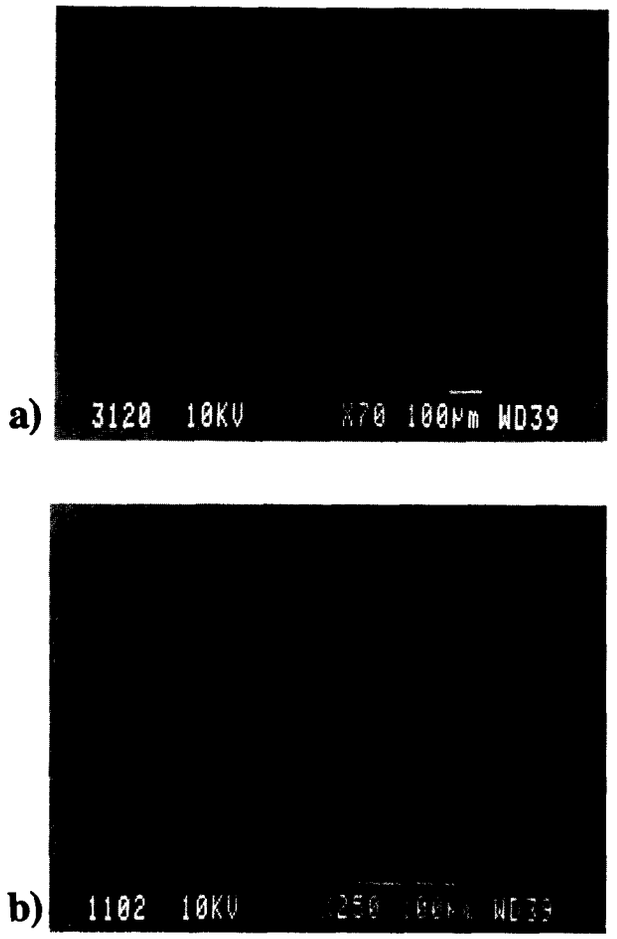

Figure 13 SEM micrographs of samples containing a weldline (perpendicular to flow view): (a) non-compatibilized blend; (b) compatibilized blend

finer dispersed phase ($d_n = 1.40\,\mu m$ and $d_v = 1.95\,\mu m$), well adhered to the matrix and with a $3000\,\mu m$ thick core (*Figure 7*).

Weldline. In this study, a detailed examination was carried out to analyse the dispersed phase structure at the weldline region (*Figure 13*). A much finer morphology compared to the rest of the sample, and an apparent reduction in the concentration of the dispersed phase, are observed. The overall behaviour is similar for systems both without (*Figure 13a*) and with (*Figure 13b*) compatibilizer, although there is a difference in the size of the dispersed phase, and the width of the weldline region. The micrograph in *Figure 13a* for non-compatibilized blends shows a weldline with a variable width, around $200\,\mu m$ in the skin, and roughly $600\,\mu m$ in the subskin. The micrograph of *Figure 13b* of the compatibilized blends gives a weldline width of approximately $200\,\mu m$. The compatibilizer leads to a reduction of the dispersed phase size ($d_n = 0.90\,\mu m$ and $d_v = 1.20\,\mu m$) and a narrowing of the weldline region compared to the weldline in the non-compatibilized blend ($d_n = 1.60\,\mu m$ and $d_v = 4.70\,\mu m$). The surface of etched microtomed samples reveals a skin, and a weldline region composed apparently of essentially pure PA6 as was observed for the skin region. The weldline does not appear to be straight, but is deformed in the subskin region where the shear is at a maximum. It is well known that the weldline is formed after two separated flow fronts meet. In other words it is formed from the skin region of two flow fronts. It will be shown in the next section that the width of the weldline region is approximately twice the thickness of the skin in the advancing melt front. Sketches representing the microstructure of the weldline in both blends without and with compatibilizer are shown in *Figures 14a* and *14b* respectively. The delineation between the weldline and non-weldline region is relatively straightforward and is based on the discontinuity between very small and very large particles.

Analysis of the flow front. It is well accepted that, in injection moulding, the mould filling is based on a fountain flow approach[23], which consists of the successive deposition of the material generated in the flow front on the mould wall forming the skin. If the melt front is separated by an insert or through a double feeding system, the reunification of the fronts will result in the formation of a weldline. Consequently the thorough analysis of the melt front will lead inevitably to a precise knowledge of the composition and morphology of both the skin and the weldline regions. For this reason short-shot experiments were performed and the results of the morphological and X.p.s. analysis of the melt front will be presented.

From the micrograph of *Figure 6b* (with compatibilizer) corresponding to position 2, the skin of the flow front is roughly $100\,\mu m$ thick. It appears that this structure is maintained all along the specimen length. If it is assumed that the skin is deposited from the melt front

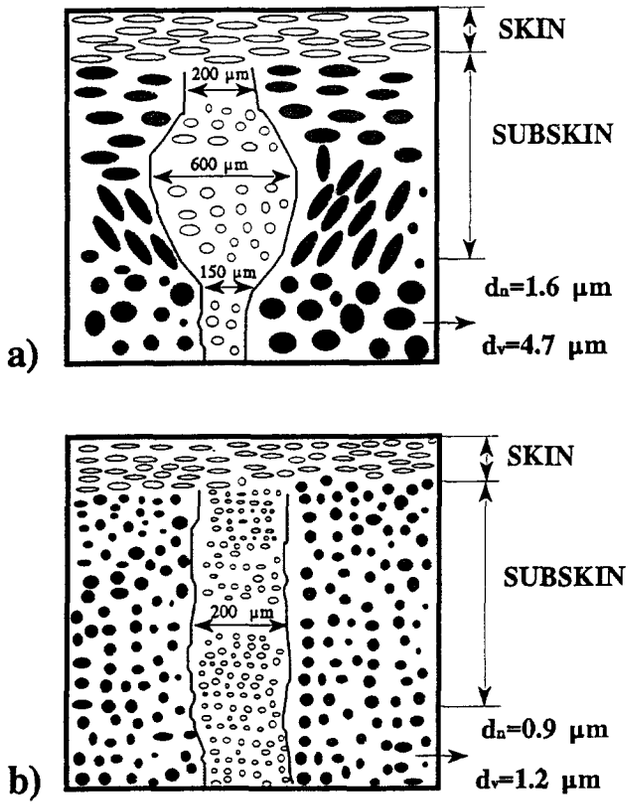

Figure 14 Schematic representation of weldline structure: (a) non-compatibilized blend; (b) compatibilized blend

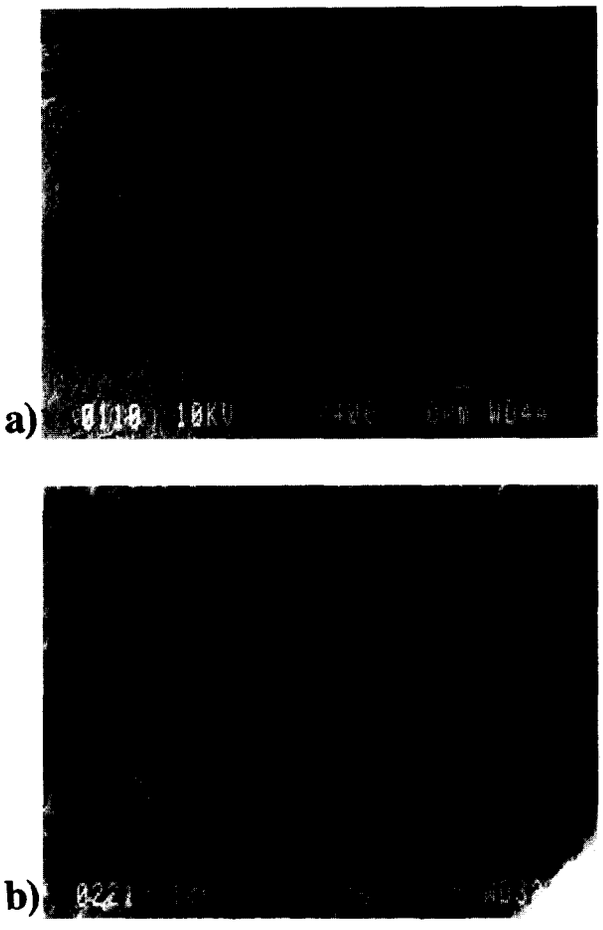

Figure 15 SEM micrographs of short-shot samples taken at position 1, and showing the skin thickness in the flow front (perpendicular to flow view): (a) with compatibilizer; (b) without compatibilizer

due to fountain flow, then a 100 μm thick skin on short-shot samples should be observed. The micrograph in *Figure 15a* shows the front in the short-shot sample having a skin of approximately 100 μm thickness.

If micrographs for a complete sample taken at position 4 (*Figure 5a* (without) and *Figure 6a* (with compatibilizer)) are compared, then for the former the skin is approximately 300 μm thick as was mentioned previously, but the latter is around 100 μm thick. The ionomer has caused a drastic reduction in the skin thickness. By way of comparison, the front in the non-compatibilized short-shot samples (*Figure 15b*) shows the presence of a skin of roughly 250 μm thickness. It is astonishing to observe that the skin thickness in the flow front does not appear to depend on position along the plaque. This implies a steady depletion and reconstitution of the skin in the melt front as it advances throughout the mould. It should also be noted that the SEM observations (*Figure 15*) again reveal an apparent absence of the minor phase in the skin of the flow front. The delineation of the skin thickness is based on the discontinuity between very small and very large particles.

It is well known that both the weldline and the skin regions are formed from the deposition of material originating from the melt flow front[23]. The melt front as it expands in a 'mushroom-like fashion' will be deposited on the cold surface of the mould forming a frozen skin. The rejoining of opposing or adjacent melt fronts leads to the formation of a weldline. An X.p.s. test was run on a short-shot sample, i.e. front (non-compatibilized blend). The spectrum is shown in *Figure 16* and the results are shown in *Table 3*. The amount of carbon atoms measured (78.6%) on the surface of a short-shot sample is similar to that found on the surface of a complete PEPA sample (77.8%). Then again using the rule of mixtures as before, one can easily predict the amount of carbon atoms in the flow front (76%), which is close to the initial, as-prepared amount of carbon atoms (78.6%). The composition of the skin in the flow front therefore is 35 wt% PE/65 wt% PA6. The larger discrepancy observed here as compared to the original, as-prepared, composition (20.4/79.6 wt%) can be attributed to experimental errors because the surface analysed in this case was very small. Nevertheless, the results clearly confirm the significant presence of dispersed phase. Since both the weldline region and the skin originate from the melt front, these data can be directly applied to the weldline region. In other words, both phases (HDPE and PA6) are present in the melt front as well as in the plaque skin of a PEPA sample as already mentioned. If it is assumed that the weldline region is the result of the contact between two melt fronts, then the melt front itself is essentially a copy of the weldline. This is convenient since it is difficult to obtain X.p.s. measurements directly at the weldline. It is evident from the above results therefore that the HDPE dispersed phase is present in the weldline region. *Figure 17* shows SEM micrographs taken at the same magnification inside and outside the weldline. Inside the weldline region, the dispersed phase particles are very fine, but in view of the above X.p.s. results apparently exist at elevated concentrations as elsewhere in the sample.

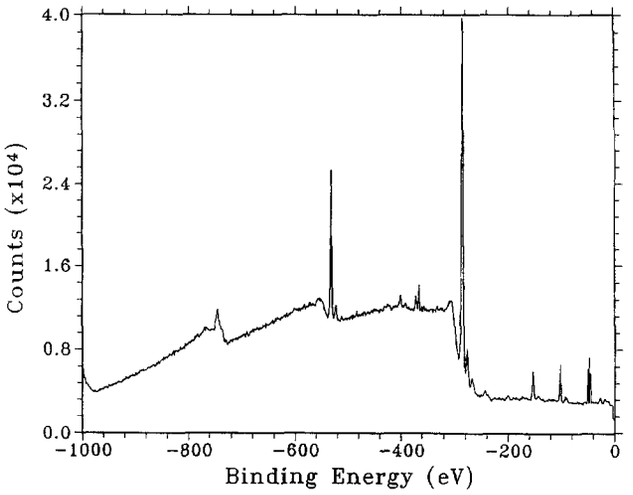

Figure 16 X.p.s. spectrum of the flow front surface of PEPA blend

These results are of significance since it has been reported on several occasions in the literature that the skin of injection-moulded polymer blends is composed of one pure component[28,29,31-33]. This work strongly indicates that great caution must be taken in the interpretation of SEM photomicrographs. In this study, it is shown that the dispersed phase is present in the skin and the weldline regions, but at significantly reduced particle dimensions. At magnification levels normally used to visualize the coarser core region, the dispersed particles in the skin become essentially invisible.

The following discussion will attempt to address the nature of the mechanism resulting in the significantly reduced size of the minor phase in both the skin and the weldline regions, as well as the morphological variations observed throughout the sample thickness. It is possible that the dispersed phase size reduction observed in the flow front and in the skin region may be attributed to particle break-up resulting from the elongational flow and biaxial stretching that the particles undergo in the melt front. This is mainly based on the 'fountain flow' effect which was introduced by Tadmor[23] to describe how polymer melts flow into an injection mould cavity. This is an inside-out flow pattern where melt streamlines in the middle of the channel, advance to the flow front, then turn outward towards the cavity wall. A schematic diagram of the flow model is shown in *Figure 4*. The melt front is stretched extensionally, which creates an oriented frontal layer that freezes upon contact with the mould surface. The fountain flow occurs in the region behind the melt front, as shown by the curved streamlines in *Figure 4*. Well behind the frontal region is laminar shear flow as shown by the parabolic velocity profile; the highest velocity being in the centre of the cavity, the lowest under the laid-down frontal layer. This velocity profile is coupled with a shear profile with a maximum shear zone located near the wall and a minimum shear zone at the middle of the channel[38].

According to this model, the orientation at the surface of the moulded part comes from the extensional orientation of the melt front and not from shear flow at the wall. Such a hypothesis is supported by the results of this study since a very fine dispersed particle size was found not only in the skin, but also in the weldline region and flow front samples. The diagram in *Figure 4* shows

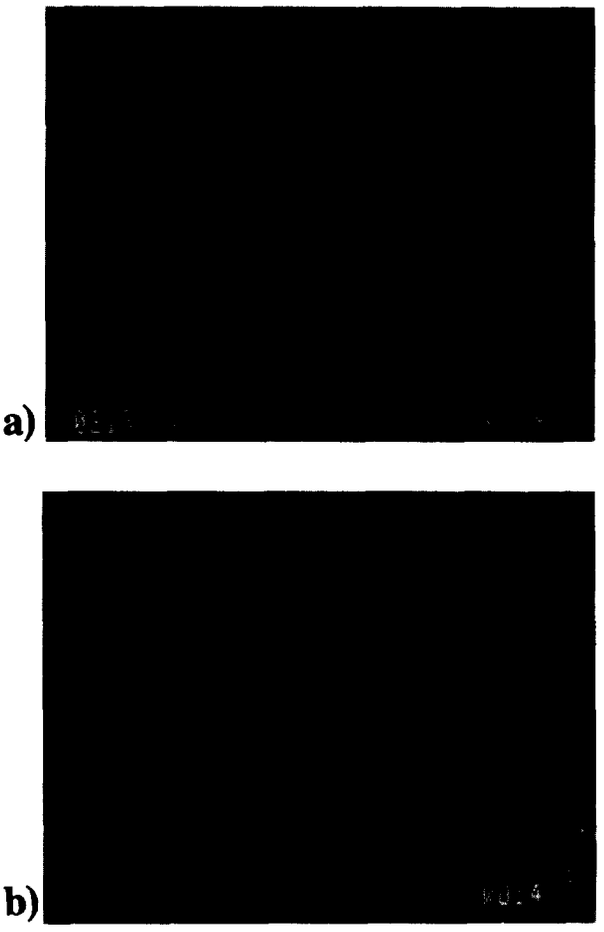

Figure 17 SEM micrographs of the weldline region in non-compatibilized blend: (a) inside the weldline; (b) outside the weldline region

that the melt elements that proceed to the very front come from the centremost streamlines where shear is at a minimum. Thus, these elements undergo an abrupt change from minimal deformation to highly stretched[37]. Similar findings have been also reported by Schmidt[40]. In addition, the theory of particle break-up seems to support the above mechanism. The critical parameters that control the particle deformation and break-up are the viscosity ratio (η_r), the shear stress ($\eta_m\dot{\gamma}$) the particle diameter (d) and the interfacial tension (σ). The basic principle of droplet deformation is that, as soon as the disruptive stress due to the viscous drag of the medium is able to overcome the cohesive effect of surface tension, the drop bursts. In previous studies on Newtonian systems it has been reported that at a high viscosity ratio ($\eta_r = 20$) the drop still bursts in an extensional flow field, whereas in uniform shear flow the drop would not burst even at the highest possible speeds. An extensional flow field is very effective for droplet break-up and the limiting viscosity ratio range is much greater than that for uniform shear flow[5].

CONCLUSION

The morphological study of injection-moulded HDPE/PA6 blends based on SEM and image analysis reveals the existence of a significant skin/core effect for the non-compatibilized blend manifested as a morphological variation with respect to the thickness, i.e. the dispersed

phase is highly oriented in the subskin and spherical in the core. Interfacial modification results in a more stable morphology displaying a reduced dispersed phase size as well as a diminution of the thickness of the skin and weldline region. An apparent absence of the minor phase in the skin and weldline regions was observed for both uncompatibilized and compatibilized blends.

To verify the validity of the above observation related to the apparent absence of the minor phase in both the skin and weldline regions, differential scanning calorimetry (d.s.c.) thermograms of microtomed slices from the skin, transmission electron microscopy (TEM) as well as X-ray photoelectron spectroscopy (X.p.s.) analysis of the surface of the blends, Surlyn and neat resins were performed. This detailed compositional analysis reveals the presence of both components (HDPE and PA6) on the surface of the plaques as well as on the melt front obtained through short-shot experiments, at approximately the same composition as in the original, as-prepared blend. When an interfacial modifier is used, X.p.s. analysis reveals values for the surface composition similar to the unmodified case.

The apparent absence of dispersed phase as observed by SEM was attributed to the very fine size of the dispersed phase in the skin relative to the core. The nature of the mechanism governing the significantly reduced size of the minor phase in both the skin and weldline region is thought to be related to particle break-up resulting from the elongational flow and biaxial stretching that the particles undergo in the melt front.

REFERENCES

1 Utracki, L. A. 'Polymer Alloys and Blends: Thermodynamics and Rheology', Hanser, Munich, 1989, Ch. 1
2 Baker, W. E. and Saleem, M. *Polym. Eng. Sci.* 1987, **27**, 1634
3 Xanthos, M. *Polym. Eng. Sci.* 1987, **28**, 1392
4 Liu, T. M., Xie, H. Q., O'Callaghan, Rudin, A. and Baker, W. E. *J. Polym. Sci. (B) Polym. Phys.* 1993, **31**, 1347
5 Favis, B. D. *Can. J. Chem. Eng.* 1991, **69**, 619
6 Chen, C. C. and White, J. L. *Polym. Eng. Sci.* 1993, **33**, 923
7 Padwa, A. R., Presented at the 11th NRCC/IMI Symposium 'Polyblends-91', Oct. 1991, Boucherville, Québec, Canada
8 Min, K., Endo, S., White, J. L., Kyu, T. and Fellers, J. F. *SPE ANTEC Tech. Pap.* 1985, **31**, 530
9 Liang, B. R., White, J. L., Spruiell, J. E. and Goswani, B. C. *SPE ANTEC Tech. Pap.* 1983, **29**, 92
10 Min, K., White, J. L. and Fellers, J. F. *Polym. Eng. Sci.* 1984, **24**, 1327
11 Chen, C. C., Fontan, E., Min, K. and White, J. L. *Polym. Eng. Sci.* 1988, **28**, 69
12 Fairley, G. and Prud'homme, R. E. *Polym. Eng. Sci.* 1987, **27**, 1495
13 Serpe, G., Jarrin, J. and Dawans, F. *Polym. Eng. Sci.* 1990, **30**, 553
14 Ghiam, F. and White, J. L. *Polym. Eng. Sci.* 1991, **31**, 76
15 Van Gheluwe, P., Favis, B. D. and Chalifoux, J. P. *J. Mater. Sci.* 1988, **23**, 3910
16 Willis, J. M., Favis, B. D. and Lavallée, C. J. *J. Mater. Sci.* 1992, **27**
17 Favis, B. D., Lavellée, C. and Derdouri, A. *J. Mater. Sci.* 1992, **27**, 4211
18 Willis, J. M. and Favis, B. D. *Polym. Eng. Sci.* 1988, **28**, 1416
19 Macknight, W. J., Lenz, R. W., Musto, P. V. and Somani, R. J. *Polym. Eng. Sci.* 1985, **25**, 1124
20 Fisa, B., SPI 46th Conference Preprints, 1991, Session 9-C
21 Gilmore, G. D. and Spencer, R. S. *Mod. Plast.* 1951, **4**, 117
22 Hagerman, E. D. *Plast Eng.* 1973, **10**, 67
23 Tadmor, Z. *J. Appl. Polym. Sci.* 1974, **18**, 1753
24 Tomari, K., Harada, T., Maekawa, Z., Hamada, H., Iwamoto, M. and Ukai, A. *Polym. Eng. Sci.* 1993, **33**, 996
25 De Gennes, P. G. *J. Chem. Phys.* 1971, **55**, 572
26 Wool, R. P., Yuan, B. L. and McGarel, O. J. *Polym. Eng. Sci.* 1989, **29**, 1340
27 Titomanlio, G., Piccarolo, S. and Rallis, A. *Polym. Eng. Sci.* 1989, **29**, 209
28 Malguarnera, S. C. and Riggs, D. C. *Polym. Plast. Tech. Eng.* 1981, **17**, 193
29 Thamm, R. C. *Rubber Chem. Technol.* 1977, **50**, 24
30 Nolley, E., Barlow, J. W. and Paul, D. R. *Polym. Eng. Sci.* 1980, **20**, 364
31 Karger-Kocsis, J. and Csikai, I. *Polym. Eng. Sci.* 1987, **27**, 241
32 Fisa, B., Bouti, A., Favis, B. D. and Lalande, F. *SPE ANTEC Tech. Pap.* 1991, **37**, 1135
33 Fellahi, S., Favis, B. D. and Fisa, B. *SPE ANTEC Tech. Pap.* 1993, **39**, 211
34 Favis, B. D. and Therrien, D. *Polymer* 1991, **32**, 1475
35 Poulin, D., Diawara, Y., Currie, J. F., Yelon, A., Gujrathi, S. C. and Petrova-Koch, V. *Mater. Res. Soc. Symp. Proc.* 1993, **283**, 88
36 Favis, B. D.and Chalifoux, J. P. *Polym. Eng. Sci.* 1987, **27**, 1591
37 Fritch, L. *Plast. Eng.* 1979, **5**, 68
38 Moulder, J. F. *et al.* 'Handbook of XPS' (Ed. J. Chastain), Perkin-Elmer, 1992, Ch. 1
39 Beamson, G. and Briggs, D. 'A Resolution XPS of Organic Polymers: Scienta ESCA 300 Data Base', Wiley, New York, 1990
40 Schmidt, L. R. *Polym. Eng. Sci.* 1974, **13**, 797